Multibeam Leaky-Wave Antenna for Mm-wave Wide-Angular-Range AoA Estimation

Julien Sarrazin, Guido Valerio

Multibeam Leaky-Wave Antenna for Mm-wave Wide-Angular-Range AoA Estimation

Julien Sarrazin*, Guido Valerio*,
*Sorbonne Université, CNRS, Laboratoire de Génie Electrique et Electronique de Paris, 75252, Paris, France
Université Paris-Saclay, CentraleSupélec, CNRS, Laboratoire de Génie Electrique et Electronique de Paris, 91192, Gif-sur-Yvette, France, julien.sarrazin@sorbonne-universite.fr

***Abstract*—The design of a periodic leaky-wave antenna for angle-of-arrival (AoA) estimation is presented. Thanks to multiple radiating space harmonics, a multibeam operation is achieved in order to scan a large angular range with a limited fractional frequency bandwidth. The matching and radiation efficiency issues raised by the large spatial period involved with multibeam operation is addressed by using a dedicated unit-cell to control both the leakage constant and the Bloch impedance. Simulations confirm that a MUSIC processing enables the system to perform AoA estimation without ambiguity among the multiple beams. This allows for AoA estimation over the 180°-angular range with a bandwidth of only 3.7% at 27 GHz.**

***Index Terms*—Leaky-wave antennas, multibeam, dielectric-filled rectangular waveguide, angle-of-arrival estimation, MUSIC.**

I. Introduction

Leaky-wave antennas (LWA) are a class of radiating devices that naturally exhibit an angular beam scanning with frequency. These properties make LWA interesting candidates to perform angle-of-estimation (AoA) estimation at millimeter-wave with a lower cost and complexity than classical systems such as phased arrays [1], [2].

However, to cover a large field of view (FoV), LWA-based AoA estimation needs to operate with a large bandwidth.

Some attempts to improve the scanning velocity at mm-wave are proposed in the literature such as loading the leaking guiding structure with a dense metasurface [3]. However, the required bandwidth to scan a large FoV remains much larger than bandwidths typically used in a given wireless communication standard. To circumvent this issue, authors have proposed the use of several multiport LWAs [4], [5] or reconfigurable LWAs [6] at the expense of increased complexity.

It was recently shown in [7] that using a multibeam operation with periodic LWAs enables to scan a large FoV with a reduced bandwidth, in the case where the sources are known and use orthogonal frequency-division multiplexing (OFDM)-type communication schemes. To achieve such an operation, the spatial periodicity of the LWA should be large enough to ensure the presence of multiple fast spatial harmonics contributing to the far field radiation. However, a large spatial period is an issue in finite-size antennas. Indeed, the number of unit-cells becomes limited thereby requiring each of them to leak a consequent amount of power to reach a satisfactory radiation efficiency. This necessitates strong discontinuities within the LWA guiding medium which in turns raises the issue of impedance matching. In fact, the small number of cells employed prevents the tapering of the cells to achieve a good input matching.

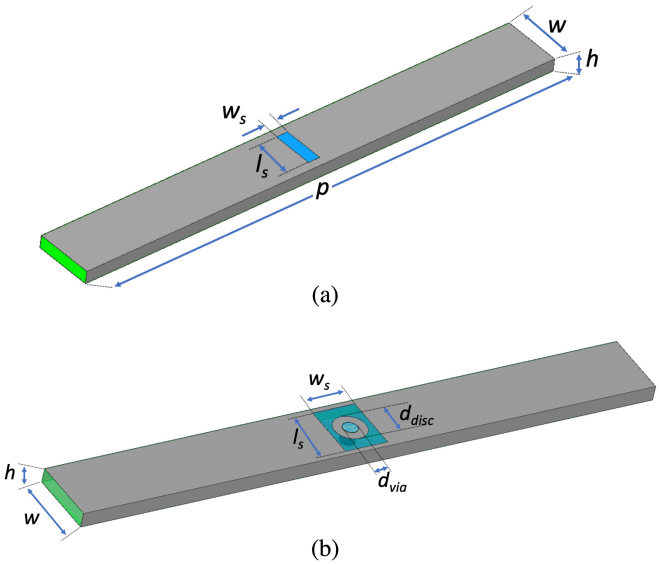

Fig. 1: Unit-cell ($w = 3.5$ mm and $h = 0.762$ mm): (a) rectangular slot; (b) rectangular slot with via hole.

To tackle this problem, the example of a slotted dielectric-filled rectangular waveguide is considered. Section II first shows the limitation of simple rectangular slots periodically etched in the waveguide in large unit cells. A new unit-cell is therefore proposed that exhibits sufficient degrees of freedom to control the leakage while maintaining a constant Bloch impedance over the frequency range of interest. Section III uses this improved unit-cell in the design of a LWA operating at 28 GHz and discusses its performance. AoA estimation using the multibeam LWA is assessed in simulation in Section IV using a frequency-domain MUSIC implementation. Conclusions of this work are drawn in Section V.

II. Unit-cell analysis

The antennas under analysis are dielectric-filled rectangular waveguides with rectangular slots periodically etched on their top plate in the transversal E plane (Figs. 1(a)-(b)). Practical millimeter-wave applications could require the implementa-

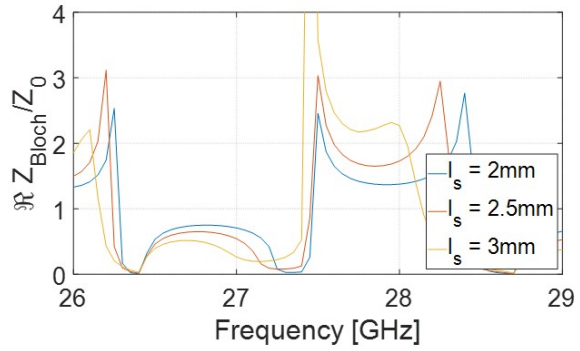

(a)

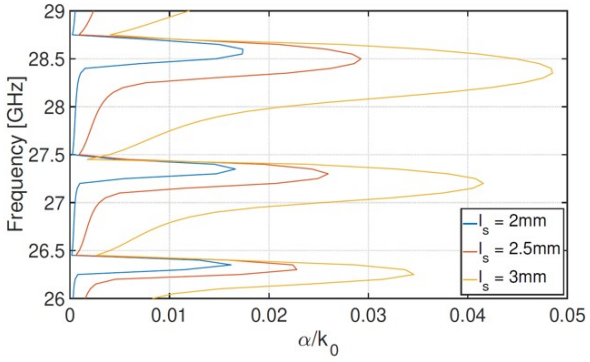

(b)

Fig. 2: Dispersive analyses of the rectangular-slot unit cell ($w_s = 0.75$ mm). (a) Real part of the normalized Bloch impedance. (b) Normalized attenuation constant.

tion of substrate-integrated waveguides or gap waveguides to facilitate the fabrication and/or to reduce losses. However in this work, a perfect metallic waveguide is assumed since the leakage mechanisms discussed here are largely independent on the choice of the technology.

Two structures are considered. A first unit cell (Fig. 1(a)) has rectangular slots of length l_s along the E plane and width w_s along the H plane, and spatial period p. In the second structure, a vertical metallic via is added in the middle of each slot topped with a metallic disc (Fig. 1(b)). In this section lossless cells are studied, while losses are introduced in the final design in following sections. The width and the height of the waveguide are set to $w = 3.5$ mm and $h = 0.762$ mm, respectively, and are fixed throughout this paper.

The complex propagation constant $k = \beta - j\alpha$ and the Bloch impedance Z_{bloch} of these structures are computed as a function of the frequency. On one hand, the propagation constant describes the phase progression (β) and the decay due to radiation (α) of the wave propagating inside the waveguide. The value of α should allow for a progressive leakage along the waveguide: an α too large prevents a uniform illumination of the entire line, while an α too small is related to an inefficient radiation [8]. On the other hand, the Bloch impedance [9] should be close to the impedance of the uniform waveguide in order to optimize the matching in the absence of an input tapering, not practical here since the truncated antenna includes few cells due to its large period. The S parameters of the unit cell are here used to obtain the complex wavenumber and the Bloch impedance of the leaky wave propagating in the waveguide [9]. Even if the multicell coupling is not taken into account [10], the results are expected to be sufficiently accurate to discuss the differences between the unit cells proposed.

The structure in Fig. 1(a) is first analysed. In Fig. 2(a) the real part of the normalized Bloch impedance Z_{Bloch}/Z_0 vs. frequency is shown (Z_0 being the impedance at the access ports) with different geometrical parameters of the slot. It is clear that, being always far from one, the line would be strongly mismatched unless a suitable tapering is introduced at both ports. In Figure 2(b) the normalized attenuation constant α/k_0 vs. frequency is shown (k_0 being the vacuum wavenumber) with the same geometrical parameters as in Fig. 2. Frequency intervals with rather high α can be observed (where an efficient illumination of the entire structure is not possible as the wave is in a stop-band regime rather than of a leaky regime) and frequency intervals with very small α (where the radiation does not occur since the slots are not radiating efficiently).

In order to overcome these issues, a vertical metallic via is added inside each slot (Fig. 1(b)) in order to compensate the capacitive effect of slots with an inductive element. In Fig. 3(a) the real part of the normalized Bloch impedance Z_{Bloch}/Z_0 can be now tuned much closer to one by acting on the size of the slot once the via dimension is fixed ($d_{via} = 0.8$ mm and $d_{disc} = 1.4$mm). This considerably improves the input matching of the line and consequently its radiation efficiency. In Figure 3(b), the normalized attenuation constant α/k_0 has a more uniform behaviour with values allowing a more uniform illumination of the structure. Note that the resonances visible as small ripples in these figures are open stop-bands of the periodic line and could be suppressed by suitably optimizing the geometry of the unit cell, but this is not discussed here for the sake of brevity.

III. Antenna Design

Based on the previous discussion, a LWA is designed and composed of six unit-cells with vias. The design parameters have been optimized and are given in Table I. Since the structure is composed of a small number of unit-cells, the design parameters differ from section II where an infinite number of unit-cells was assumed. The waveguide is filled with Rogers RT Duroid 6002 (thickness $h = 0.762$ mm) and its overall length is 18.78 cm. The LWA is simulated with Ansys HFSS.

Fig. 4 shows the magnitude of the S parameters of the antenna. The magnitude of the S_{11} confirms that a good matching is obtained in the entire band 26-29 GHz apart a small mismatch around 28 GHz. The magnitude of the lossless

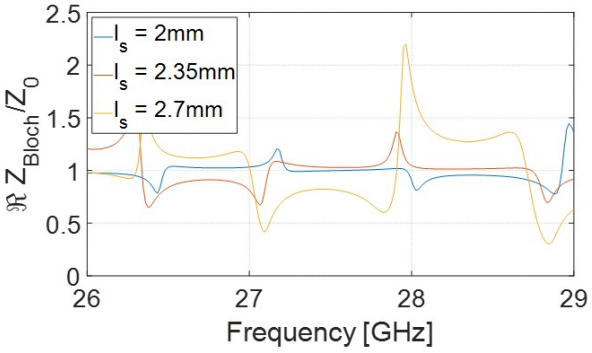

(a)

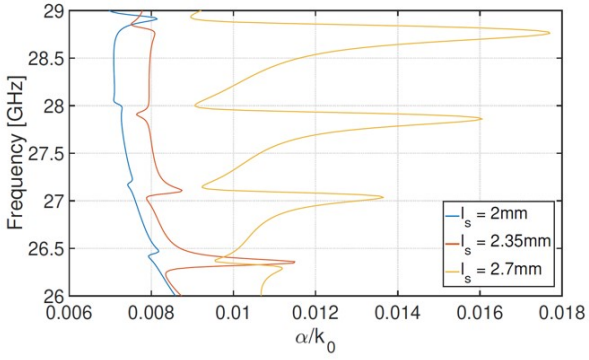

(b)

Fig. 3: Dispersive analyses of the rectangular slot unit-cell with vertical via. Parameters: $l_s = 2$ mm and $w_s = 2.4$ mm (*blue lines*), $l_s = 2.35$ mm and $w_s = 1.75$ mm (*red lines*), $l_s = 2.7$ mm and $w_s = 1.5$ mm (*yellow lines*). (a) Real part of the normalized Bloch impedance. (b) Normalized attenuation constant.

TABLE I: 6-unit-cells LWA Design Parameters

ϵ_r	$\tan\delta$	p	l_s	w_s	d_{via}	d_{disc}
2.94	0.0012	31.3mm	3mm	2.3mm	0.8mm	1.7mm

S_{21} shows that the power has leaked into free space before reaching the output port as desired. The presence of losses reduced the power reaching the second port by about 5 dB, thus lowering of the same amount the radiated power. The radiation pattern is shown in Fig. 5. The expected multiple beams are consistent with the visible harmonics defined by the period and the phase constant of the leaky wave (not shown here for brevity). Each radiating harmonic has a different amplitude, which leads to radiated beams having different amplitudes. The typical frequency scanning of LWAs is observable when varying the frequency 26 to 28 GHz.

IV. AoA Estimation Results

A. MUSIC system model

The AoA estimation of D received signals is performed using MUSIC algorithm. The D sources are considered to be

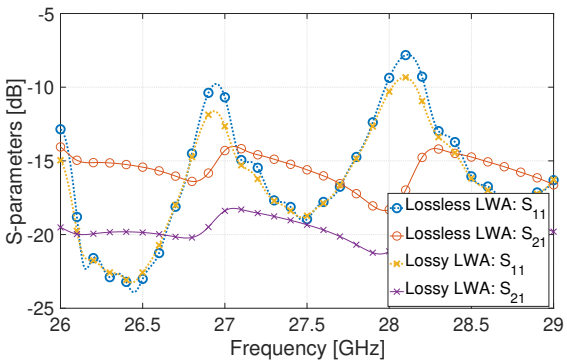

Fig. 4: S-parameters of the LWA composed of 6 unit-cells as shown in Fig. 1(b) with dimensions given in Table I.

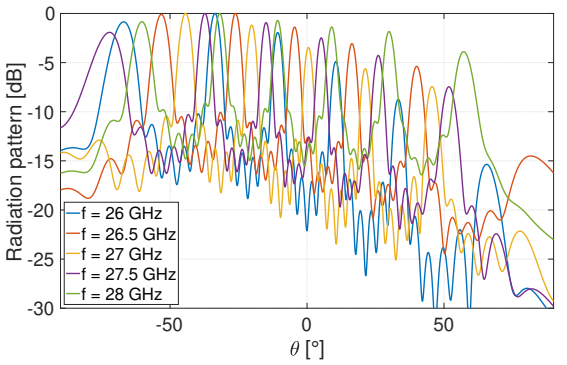

Fig. 5: Radiation pattern of the lossless 6-unit-cell LWA .

modulated using a multicarrier scheme such as OFDM. Further assuming that signals on each subcarrier are identical, it is then possible, under narrow-band approximation, to construct a frequency-domain system model similar to spatially-sampled MUSIC to express the received signal due to D plane waves impinging on the LWA, here in one angular plane only:

$$\begin{bmatrix} x_1[n] \\ \vdots \\ x_M[n] \end{bmatrix} = \begin{bmatrix} a_1(\theta_1) & \dots & a_1(\theta_D) \\ \vdots & \ddots & \vdots \\ a_M(\theta_1) & \dots & a_M(\theta_D) \end{bmatrix} \cdot \begin{bmatrix} s_1[n] \\ \vdots \\ s_D[n] \end{bmatrix} + \begin{bmatrix} z_1[n] \\ \vdots \\ z_M[n] \end{bmatrix} \quad (1)$$

with $\mathbf{x} \in \mathbb{C}^{M\times 1}$, the received data vector, $\mathbf{A} \in \mathbb{C}^{M\times D}$, the LWA response matrix, $\mathbf{s} \in \mathbb{C}^{D\times 1}$, the source vector, $\mathbf{z} \in \mathbb{C}^{M\times 1}$, a complex Additive White Gaussian Noise (AWGN) vector with uncorrelated components, and $n = 1, \dots, N$ is the OFDM symbol index (i.e., the nth snapshot among N). M is the number of frequency samples, i.e., number of OFDM subcarriers, as opposed to the number of single antenna elements in a more traditional spatially-sampled MUSIC approach. Each column of $\mathbf{A}$ represents the LWA response of an incoming plane wave whose AoA is $\theta_{i=1,\dots,D}$ and is given by the HFSS simulations shown in previous section.

From the system model in (1), an estimation of the covariance matrix of the received signal $\mathbf{x}$ can be calculated, from

which the MUSIC pseudo spectrum is determined. Furthermore, the standard deviation of the MUSIC estimator can be derived as in [7], [11].

B. Results and performance

Unless stated otherwise, $f_0 = 27$ GHz (central frequency), $\Delta_f = 2$ GHz (i.e., fractional bandwidth of 7.4%), $M = 201$ frequency samples, $N = 500$ snapshots, and SNR = 10 dB. The antenna used for AoA estimation is the LWA presented in section III.

The MUSIC pseudo spectrum is first shown in Fig. 6 with $D = 3$ uncorrelated sources. Two sets of AoAs are considered: $\mathbf{\Theta_A}$: $\{\theta_1 = -32°, \theta_1 = -20°, \theta_3 = 68°\}$ and $\mathbf{\Theta_B}$: $\{\theta_1 = -38°, \theta_1 = -37°, \theta_3 = 10°\}$. It is first observed that in all cases, the highest peaks correspond accurately to the AoAs. Some lower spurious peaks exist due to the similarity exhibited by the LWA multiple beams. With the $\mathbf{\Theta_A}$ set of AoA (blue curve), the peak for $\theta_3 = 68°$ is less sharp, which is due to the wide beamwidth exhibited by the LWA when scanning towards end-fire directions. In the $\mathbf{\Theta_B}$ set of AoA (red curve), two close sources (θ_1 and θ_2) are successfully distinguished in the pseudo spectrum. Their 1°-angular distance is less than the 4.1°-half-power beamwidth of the LWA in this angular region. When the operating bandwidth is decreased to 1 GHz ($\Delta_f/f_0 = 3.7\%$, black curve), the AoAs are still successfully identified but the spurious peaks level increases. Increasing the SNR and/or the number of snapshots decreases the level of those spurious peaks (not shown here).

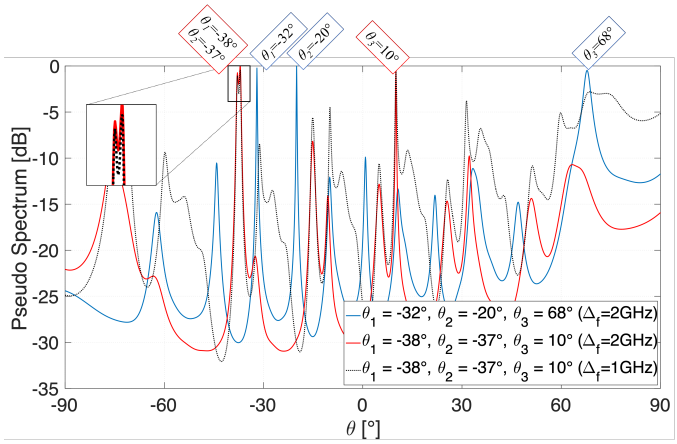

Fig. 6: Normalized MUSIC pseudo-spectrum (SNR = 10 dB, $M = 201$, $N = 500$.

The standard deviation is shown in Fig. 7 as a function of the AoA of a single source. Performance are compared with $\lambda/2$-spaced-antenna arrays. It is shown that when $M = 201$ frequency samples are used, the performance of the LWA is mostly similar to that of a 4-antenna array. As expected, when the number of samples increases, the standard deviation decreases. Increasing M with the LWA corresponds to increasing the number of frequency samples, that is the number of subcarriers, which comes at practically no additional cost. However, increasing M with an antenna array translates in

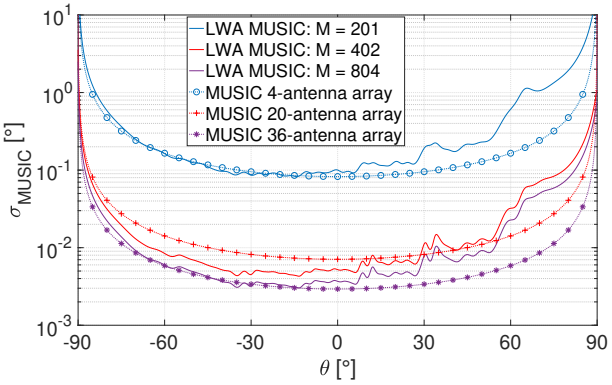

Fig. 7: Standard deviation in [°] (SNR = 10 dB, $N = 500$, $f_0 = 27$ GHz, $\Delta_f = 2$ GHz.

increasing the number of antenna elements. Therefore, it is shown that an AoA estimation with the proposed scheme using a single LWA, can exhibit performance in terms of standard deviation similar to that of a 20-antenna and 36-antenna array when $M = 402$ and $M = 804$ respectively. It is to be noted that the LWA performance tends to decrease faster than those of the antenna array as the AoA approaches angles close to $+90°$. However, this is related to the fact that the antenna array simulation considers perfect isotropic antennas as single elements, and therefore does not take into account the gain decay typically observed toward end-fire directions.

V. Conclusion

This paper introduces the design of a multibeam leaky-wave antenna (LWA) to perform angle-of-arrival (AoA) estimation thanks to frequency beam scanning in the 28 GHz band. Multibeam operation enables scanning a wide angular range with a limited frequency bandwidth. Multiple radiating beams are achieved thanks to several fast spatial harmonics in a dielectric-filled rectangular waveguide etched with periodic slots. The large spatial period required for multibeam operation leads to leakage constant values too small to reach a decent radiation efficiency with finite-size LWA. This issue is overcome by the introduction of a new unit-cell composed of a rectangular slot and a vertical metallic via. A 6-unit-cell multibeam LWA is designed and numerical simulations show that, combined with a frequency-domain MUSIC processing, it can estimate AoAs over the entire 180° angular range with no ambiguity among the multiple beams using a fractional bandwidth as low as 3.7%. This approach is promising in order to perform real-time AoA estimation with a low-complexity system using bandwidths compatible with wireless communication standards.

Acknowledgment

This work was performed within the NOVIS60 project supported by the CEFPRA (Indo-French Center for the Promotion of Advanced Research) and carried out in the framework of COST Action CA20120 INTERACT.

REFERENCES

[1] C. U. Bas et al., "Real-Time Millimeter-Wave MIMO Channel Sounder for Dynamic Directional Measurements," IEEE T-VT, 68, 9, Sept. 2019, pp. 8775–8789, doi: 10.1109/TVT.2019.2928341.

[2] Z. Guo, X. Wang and W. Heng, "Millimeter-Wave Channel Estimation Based on 2-D Beamspace MUSIC Method," in IEEE Trans. on Wireless Communications, vol. 16, no. 8, pp. 5384-5394, Aug. 2017, doi: 10.1109/TWC.2017.2710049.

[3] Q. Zhang, J. Sarrazin, M. Casaletti, G. Valerio, P. De Doncker, A. Benlarbi-Delai, "Enhanced Scanning Range Design for Leaky-Wave Antenna (LWA) at 60 GHz", 13th European Conference on Antennas and Propagation (EuCAP), Krakow, Poland, 1-5 April 2019

[4] M. K. Emara, D. J. King, H. V. Nguyen, S. Abielmona, and S. Gupta, "Millimeter-Wave Slot Array Antenna Front-End for Amplitude-Only Direction Finding," in IEEE Trans. on Antennas and Propagation, vol. 68, no. 7, pp. 5365-5374, July 2020, doi: 10.1109/TAP.2020.2979284.

[5] M. Poveda-García, A. Gómez-Alcaraz, D. Cañete-Rebenaque, A. S. Martinez-Sala and J. L. Gómez-Tornero, "RSSI-Based Direction-of-Departure Estimation in Bluetooth Low Energy Using an Array of Frequency-Steered Leaky-Wave Antennas," in IEEE Access, vol. 8, pp. 9380-9394, 2020, doi: 10.1109/ACCESS.2020.2965233.

[6] H. Paaso, et Al., "DoA estimation through modified unitary MUSIC algorithm for CRLH leaky-wave antennas," IEEE PIMRC, London, 2013, pp. 311-315, doi: 10.1109/PIMRC.2013.6666152.

[7] J. Sarrazin, "MUSIC-based Angle-of-Arrival Estimation using Multi-beam Leaky-Wave Antennas," URSI GASS 2021, Rome, Italy, 28 August - 4 September 2021

[8] J. Volakis, *Antenna Engineering Handbook*, 4th ed. New York, NY, USA: McGraw-Hill, 2007.

[9] D. M. Pozar, "Microwave filters," in *Microwave Engineering*. Hoboken, NJ, USA: Wiley, 2011, ch. 8.

[10] G. Valerio, S. Paulotto, P. Baccarelli, P. Burghignoli, and A. Galli, "Accurate Bloch analysis of 1-D periodic lines through the simulation of truncated structures," *IEEE Trans. Antennas Propag.*, vol. 59, no. 6, pp. 2188–2195, Jun. 2011.

[11] P. Stoica and A. Nehorai, "MUSIC, maximum likelihood, and Cramer-Rao bound," IEEE T-ASSP, 37, 4, May 1989, pp. 720-741, doi: 10.1109/29.17564.